Available online at www.sciencedirect.com
SCIENCE DIRECT®
Journal of Sound and Vibration 288 (2005) 1105–1130
JOURNAL OF SOUND AND VIBRATION
www.elsevier.com/locate/jsvi

Adaptive Helmholtz resonators and passive vibration absorbers for cylinder interior noise control

Simon J. Estève*, Marty E. Johnson

Vibration and Acoustics Laboratories Virginia Tech, Blacksburg, VA 24061-0238, USA

Received 21 June 2004; received in revised form 5 January 2005; accepted 25 January 2005
Available online 31 March 2005

Abstract

This paper presents an adaptive-passive solution to control the broadband sound transmission into rocket payload fairings. The treatment is composed of passive distributed vibration absorbers (DVAs) and adaptive Helmholtz resonators (HR). Both the frequency domain and time-domain model of a simply supported cylinder excited by an external plane wave are developed. To tune vibration absorbers to tonal excitation, a tuning strategy, based on the phase information between the velocity of the absorber mass and the velocity of the host structure is used here in a new fashion to tune resonators to peaks in the broadband acoustic spectrum of a cavity. This tuning law, called the dot-product method, only uses two microphone signals local to each HR, which allows the adaptive Helmholtz resonator (AHR) to be manufactured as an autonomous device with power supply, sensor, actuator and controller integrated. Numerical simulations corresponding to a 2.8 m long 2.5 m diameter composite cylinder prototype demonstrate that, as long as the structure modes, which strongly couple to the acoustic cavity, are damped with a DVA treatment, the dot-product method tune multiple HRs to a near-optimal solution over a broad frequency range (40–160 Hz). An adaptive HR prototype with variable opening is built and characterized. Experiments conducted on the cylinder prototype with eight AHRs demonstrate the ability of resonators adapted with the dot-product method to converge to near-optimal noise attenuation in a frequency band including multiple resonances.

*Corresponding author. Tel.: +1 540 231 8028; fax: +1 540 231 8836.
E-mail address: sesteve@vt.edu (S.J. Estève).

0022-460X/$ - see front matter © 2005 Elsevier Ltd. All rights reserved.
doi:10.1016/j.jsv.2005.01.017

1. Introduction

In an attempt to increase payload size and increase efficiency, aerospace structures have become progressively lighter. One drawback to this development is a decrease in broadband low-frequency transmission loss where passive sound absorption treatments are very ineffective. One solution is to apply optimally damped Helmholtz Resonators (HRs) to increase the acoustic damping of the enclosure, and optimally damped distributed vibration absorbers (DVAs) to increase the damping of the structure. This method has been investigated theoretically [1,2] and has recently been tested experimentally [3]. The results of these tests show that multiple HRs effectively reduce the overall sound pressure level inside a lightly damped cylinder that is excited with a high-level external sound source. Optimally damped DVAs, provide further noise attenuations by reducing the amplitude of structural modes, that couple well to the interior cavity. For a HR/DVA treatment to be effective, these devices must be tuned so that they interact with the acoustic/structural modes of the cylinder. In this paper, tunable HRs are designed and a control scheme is developed in order to tune the HR to the natural frequencies of a cavity which change with different payload fills. This work represents an improvement from the simply passive treatment presented in Ref. [1] into an adaptive-passive treatment.

To improve the performance of passive treatments and especially to increase their robustness to uncertainty and to changes in the excitation frequency or in the system's characteristics, adaptive-passive methods have been developed. Adaptive-passive treatments are made of passive devices such as dynamic vibration absorbers or HRs, which cannot inject energy in the system they are implemented in. Thus, they rarely increase the system's overall energy as opposed to active control treatments. As mentioned by Bernhard [4], most effective adaptive passive solutions have been developed for narrow frequency band applications where they provide a great advantage over active control means in terms of cost and power consumption and over passive treatments in term of robustness. Several authors have constructed resonators whose tuning frequency is modified by varying the volume of the HR's cavity [5–7] or by varying the opening area [8]. All of this research involves the tuning of a single device using gradient-based search algorithm or feedback control scheme to minimize a tonal excitation at one error microphone. In contrast, this paper presents multiple devices that adapt to changes in the natural frequencies of the system under broadband excitation in order to lead to global noise reduction. For the global control of structural vibration under single-frequency excitation, Dayou et al. [9] investigated the use of multiple-tuned vibration absorbers. To avoid complex tuning algorithms, and numerous sensors to estimate global vibration, the absorbers are tuned to the excitation frequency using a simple local control strategy [10,11], This tuning strategy, called the dot-product or (or cross-product) method uses the phase information between the velocity of the absorber mass and the velocity of the host structure. It has recently been shown [12] theoretically that when applied to multiple absorbers, this method, can lead to good broadband attenuation in a lightly damped modal system. Here, this method is applied to HRs and is extended to a realistic noise transmission scenario where the adaptive devices are used to control the sound transmission into a large composite cylinder excited by a broadband external noise source. The effect of the structural excitation is therefore taken into account. Under this tuning law the HRs can track changes in the acoustic spectrum provoked by varying payloads fills. This control strategy also uses information that is purely local to each device, namely the pressure inside the HR cavity and the pressure outside the throat, and is

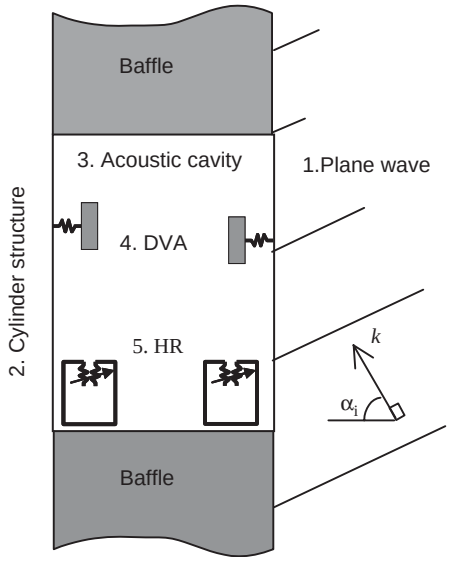

Fig. 1. Schematic of a simply supported cylinder embedded in an infinite rigid baffle, excited by an oblique plane wave of elevation angle α_i, and treated with DVAs and adaptive HRs.

therefore more practical than global strategies. Indeed, each device is independent and can be manufactured as a generic device with power supply, controller, actuator and sensor integrated.

The system studied here is represented in Fig. 1. The paper is organized as follows. Section 2 of this paper consists of the mathematical model which is composed of five parts: (1) the incident random noise and the diffraction around the cylinder, (2) the modal model of the cylindrical structure assuming simply supported boundary conditions, (3) the modal model of the acoustic cavity, (4) the coupling between the passive DVAs and the structure, and (5) the interaction of the HRs with the cylindrical cavity. The entire system is represented in the frequency domain [1] by coupling together two modal models. In the time-domain, it is described using a state-space approach with the appropriate forcing functions (including diffraction of the incident field) applied to the states of the system.

In Section 3, the dot-product method and its mechanisms for both single frequency and broadband excitation is presented. Then, in Section 4, numerical simulations show the real-time adaptation of the HRs in a single and multi-mode case.

To validate the numerical simulations, experimental results conducted on a 2.8 m long 2.5 m diameter composite cylinder are presented in Section 5. The characteristics of developed adaptive HR prototype as well as the controller used in this experiment are detailed. Some conclusions are given in Section 6.

2. Mathematical model

The theoretical model presented here is based on the coupling of a structural modal model to a modal model of the acoustic cavity. The DVAs and the HRs are coupled to the structural and the

acoustic model, respectively, using an impedance matching method. As the frequency model has been presented in detail in Ref. [1], the derivations used to obtain the different elements of the system are omitted here and only the architecture of the model leading to its matrix formulation is presented. However, the time-domain model of the system not presented in Ref. [1] is derived in detail.

2.1. Frequency domain model

Considering the system described in Fig. 1, the velocity amplitude vector of the structural modes $\mathbf{v}$ can be expressed as

$$\mathbf{v} = \mathbf{A}^s\mathbf{f} = \mathbf{A}^s(\mathbf{f}^{\text{ext}} + \mathbf{f}^{\text{dva}} + \mathbf{f}^{\text{int}}), \tag{1}$$

where $\mathbf{A}^s$ is the diagonal matrix of modal mobility of the cylinder (includes resonance term), $\mathbf{f}^{\text{ext}}$ is the external modal force vector due to the incident acoustic plane wave, $\mathbf{f}^{\text{dva}}$ is the force vector exerted by the DVA treatment and $\mathbf{f}^{\text{int}}$ is the internal modal force vector due to the acoustic pressure in the cavity. The external modal force ($\mathbf{f}^{\text{ext}}$) is obtained by integrating the product of pressure distribution created by the incident plane wave and the structural mode shape over the surface of the cylinder. This external forcing includes the diffraction of the plane wave by the rigid cylinder [1]. The reacting force exerted by the DVAs ($\mathbf{f}^{\text{dva}}$) is a function of the location and the dynamics of the device, and can be expressed as

$$\mathbf{f}^{\text{dva}} = (\mathbf{\Phi}^S)^{\text{T}} Z_d \mathbf{\Phi}^S \mathbf{v}, \tag{2}$$

where $\mathbf{Z}_d$ is the diagonal matrix of the DVA impedances, that are a function of the mass, tuning frequency and damping ratio of the DVA [1]. A DVA is a particular design of dynamic vibration absorber consisting in a distributed spring made of acoustic foam on top of which is glued a distributed mass layer. When the structural wavelength is much larger than the footprint of the DVA, this device acts mainly as a point vibration absorber and is assumed to exert a uniformly distributed force to the structure it is attached to. Therefore, it is modeled as a single degree of freedom (dof) system. Nevertheless, the larger and variable DVA footprint represents an advantage over the point absorber as it reduces stress concentration at the attachment surface and allows a more compact device. The fully populated matrix $\mathbf{\Phi}^S$ in Eq. (2) represents the spatial coupling between multiple DVAs and the structure. Each element of this structure–DVA coupling matrix is obtained by integrating the cylinder structural mode shape over the footprint of the DVA [1]. The superscript 'T' denotes the transpose. Neglecting the external fluid loading on the cylinder wall and combining Eqs. (1) and (2) yields the velocity amplitude vector of the structural modes,

$$\mathbf{v} = [\mathbf{I} - \mathbf{A}^s\mathbf{\Phi}^{s\text{T}}\mathbf{Z}_d\mathbf{\Phi}^s]^{-1}\mathbf{A}^s(\mathbf{f}^{\text{ext}} + \mathbf{f}^{\text{int}}). \tag{3}$$

The coupling coefficient $C_{i,j}$ between the ith structural mode and the jth acoustic mode is computed by integration of the product of their shape [1] over the cylinder wall. The resulting matrix $\mathbf{C}$ is the link between the structure and the acoustic cavity. By means of its physical dimension (m^2), it converts the structural modal velocity vector $\mathbf{v}$ into an modal acoustic source strength vector, $\mathbf{u}^s$:

$$\mathbf{u}^s = \mathbf{C}\mathbf{v}. \tag{4}$$

Conversely, the coupling matrix **C** converts the pressure mode amplitude vector **p** of the acoustic modes into the internal modal force vector $\mathbf{f}^{\text{int}}$ introduced in Eq. (1):

$$\mathbf{f}^{\text{int}} = -\mathbf{C}^{\text{T}}\mathbf{p}. \tag{5}$$

The pressure amplitude vector **p** is expressed as

$$\mathbf{p} = \mathbf{A}^{a}\mathbf{u} = \mathbf{A}^{a}(\mathbf{u}^{s} + \mathbf{u}^{r}), \tag{6}$$

where $\mathbf{A}^{a}$ is the diagonal matrix of modal acoustic impedances of the cavity (includes resonance term) and $\mathbf{u}^{r}$ is the acoustic modal source strength created by the HRs. The admittance of a HR defined as the ratio of the volume velocity to a unit pressure at the HR opening is derived using the single dof mechanical analog illustrated in Fig. 2. In order to provide broadband vibration and acoustic attenuation the DVAs and HRs are optimally damped [1]. Therefore, using a viscous damping model, damping ratios, ζ_h and ζ_d are implemented in the HR admittance and DVA impedance respectively. The damping of a HR is mainly caused by energy dissipation of the air in motion and can therefore be adjusted by placing acoustic screens across the resonator opening. Assuming a uniform acoustic velocity distribution across the opening, the radiation loading is taken into account by adding an interior and exterior neck correction factor δ_i and δ_e that are expressed as [13]

$$\delta_i = \delta_e = 0.48\sqrt{s_h}, \tag{7}$$

when the HR opening cross-sectional area s_h is assumed to be small compared to the cross section of the HR cavity. However, only the interior neck correction factor is included in this model as the external radiation loading is accounted for in the coupling with the cylinder cavity. Under this assumption, a HR behaves like a piston source. Thus, the coupling coefficient between a HR and the cavity is obtained by integrating the acoustic mode shape over the HR opening. These coefficients are grouped in the fully populated acoustic–HR coupling matrix $\mathbf{\Phi}^{a}$ and the acoustic modal source strength $\mathbf{u}^{r}$ created by the HRs is given by

$$\mathbf{u}^{r} = (\mathbf{\Phi}^{a})^{\text{T}}\mathbf{Y}_{h}\mathbf{\Phi}^{a}\mathbf{p}, \tag{8}$$

where $\mathbf{Y}_h$ is the diagonal matrix of HR admittances.

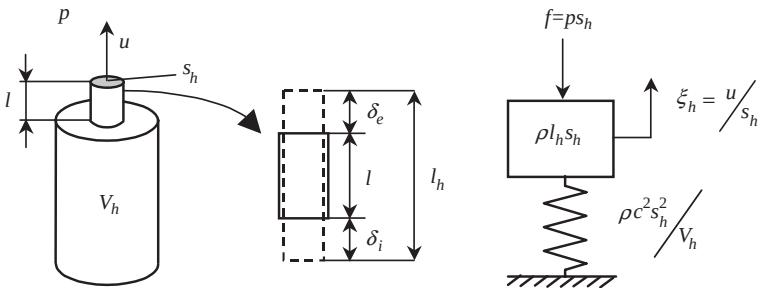

Fig. 2. Schematic and mechanical analog of a HR exposed to an external acoustic pressure p and through whose neck flows a volume velocity u.

Thus, the HR-coupled modal acoustic pressure vector $\mathbf{p}$ is expressed as

$$\mathbf{p} = [\mathbf{I} - \mathbf{A}^a \mathbf{\Phi}^{a\mathrm{T}} \mathbf{Y}_h \mathbf{\Phi}^a]^{-1} \mathbf{A}^a \mathbf{C} \mathbf{v}. \tag{9}$$

Combining Eqs. (3) and (9), the fully coupled velocity and acoustic response are given by

$$\begin{aligned} \mathbf{v} &= [\mathbf{I} + \mathbf{A}^s \mathbf{C}^{\mathrm{T}} [\mathbf{I} - \mathbf{A}^a \mathbf{\Phi}^{a\mathrm{T}} \mathbf{Y}_h \mathbf{\Phi}^a]^{-1} \mathbf{A}^a \mathbf{C} - \mathbf{A}^s \mathbf{\Phi}^{s\mathrm{T}} \mathbf{Z}_d \mathbf{\Phi}^s]^{-1} \mathbf{A}^s \mathbf{f}^{\mathrm{ext}}, \\ \mathbf{p} &= [\mathbf{I} - \mathbf{A}^a \mathbf{\Phi}^{a\mathrm{T}} \mathbf{Y}_h \mathbf{\Phi}^a]^{-1} \mathbf{A}^a \mathbf{C} \mathbf{v}. \end{aligned} \tag{10}$$

In this study, to simplify the time-domain formulation and obtain reasonable computational time, the acoustic back coupling onto the structure represented by the internal forcing $\mathbf{f}^{\mathrm{int}}$ is neglected. This simplification introduces some discrepancies in the system structural and acoustic response. However, these discrepancies remain small as long as the structure density is far greater than the air density. Under this assumption, the system then becomes one-way coupled and the structure is independent of the acoustic cavity dynamics. Therefore, the vibration response is simplified to structural modes only whereas the acoustic response of the cavity remains a mix of acoustic and structural resonances. The vibration and acoustic response simplifies then to

$$\begin{aligned} \mathbf{v} &= [\mathbf{I} - \mathbf{A}^s \mathbf{\Phi}^{s\mathrm{T}} \mathbf{Z}_d \mathbf{\Phi}^s]^{-1} \mathbf{A}^s \mathbf{f}^{\mathrm{ext}}, \\ \mathbf{p} &= [\mathbf{I} - \mathbf{A}^a \mathbf{\Phi}^{a\mathrm{T}} \mathbf{Y}_h \mathbf{\Phi}^a]^{-1} \mathbf{A}^a \mathbf{C} [\mathbf{I} - \mathbf{A}^s \mathbf{\Phi}^{s\mathrm{T}} \mathbf{Z}_d \mathbf{\Phi}^s]^{-1} \mathbf{A}^s \mathbf{f}^{\mathrm{ext}}. \end{aligned} \tag{11}$$

In order to obtain an average sound pressure level independent of the location inside the cylinder, the total time average acoustic potential energy E_p, is used and computed from the pressure mode amplitude as [14]

$$E_p = \frac{V}{4\rho c^2} \mathbf{p}^{\mathrm{H}} \mathbf{p}, \tag{12}$$

where V is the volume of the cavity, ρ the air density, c the velocity of sound in air and the superscript 'H' denotes the Hermitian transpose. Similarly, the total kinetic energy is used as an indicator of the average vibration level of the structure and is expressed as

$$E_k = \tfrac{1}{2} M \mathbf{v}^{\mathrm{H}} \mathbf{v}, \tag{13}$$

where M is the mass of the cylinder. In the next section, the time-domain model of this one way coupled system is derived.

2.2. Time-domain model

In order to simulate the real-time tuning of the resonators, the equations of the system described in Fig. 1 needs to be expressed in the time domain. Fahy and Schofield [15] describe the behavior of an enclosed fluid by

$$\nabla^2 p - \frac{1}{c^2} \frac{\partial^2 p}{\partial t^2} = -\rho \frac{\partial q}{\partial t},$$

where q is the acoustic source strength density distribution within the volume and on the surface of the enclosure. For the time-domain derivation, the acoustic velocity potential φ is introduced

and is related to the acoustic pressure p by

$$p(\mathbf{r}, t) = -\rho\dot{\varphi}(\mathbf{r}, t). \tag{14}$$

The dot indicates the differentiation with respect to time and $\mathbf{r}$ is the spatial vector regrouping the coordinates. The governing equation then becomes

$$\nabla^2\varphi - \frac{1}{c^2}\ddot{\varphi} = q(\mathbf{r}, t). \tag{15}$$

The acoustic velocity potential can be expanded in terms of the pressure modes shape of the acoustic cavity Ψ^a:

$$\varphi(\mathbf{r}, t) = \sum_N a_N(t)\Psi_N^a(\mathbf{r}), \tag{16}$$

where $a_N(t)$ is the amplitude and Ψ_N^a is the shape of the Nth acoustic mode which satisfies the homogeneous wave equation:

$$(c^2\nabla^2\Psi_N^a - \tilde{\omega}_N^2\Psi_N^a)a_N = 0, \tag{17}$$

where $\tilde{\omega}_N$ is the complex natural frequency of mode N. Using hard wall boundary conditions, the acoustic modes are assumed to be orthogonal and therefore multiplying Eq. (16) by $\Psi_{N'}^a$ and integrating it over the volume isolates each mode N:

$$V\Lambda_N(\ddot{a}_N - \tilde{\omega}_N^2 a_N) = -c^2\int_V \Psi_N^a(\mathbf{r})q(\mathbf{r}, t)\,\mathrm{d}V, \tag{18}$$

where Λ_N is the normalization factor given by

$$\Lambda_N = \frac{1}{V}\int_V [\Psi_N^a]^2(\mathbf{r})\,\mathrm{d}V.$$

The acoustic forcing on the right-hand side of Eq. (18) is composed of the forcing due to the vibration of the cylinder wall Q_N, and the forcing due to the HRs Q_N^r as

$$\int_V \Psi_N^a(\mathbf{r})q(\mathbf{r}, t)\,\mathrm{d}V = Q_N + Q_N^r. \tag{19}$$

The primary forcing Q_N is expressed as

$$Q_N = \int_s \Psi_N^a(\mathbf{r})\sum_{N_s}\Psi_{N_s}^s(\mathbf{r})v_{N_s}\,\mathrm{d}S = \sum_{N_s} C_{N,N_s}v_{N_s}, \tag{20}$$

where v_{N_s} is the velocity amplitude of the N_s structural mode $\Psi_{N_s}^s$ and C_{N,N_s} is the Nth, N_sth element of the coupling matrix $\mathbf{C}$. The term Q_N is the time-domain version of an element of the modal acoustic source strength vector $\mathbf{u}^s$ introduced in Eq. (4). The excitation of the system can also be provided by an acoustic source placed inside the cavity. The modal acoustic forcing created by a piston source of velocity v_s at $\mathbf{r}_s$ inside the cavity is then given by

$$Q_N^s = \left(\int_{s_s} \Psi_N^a(\mathbf{r}_s)\,\mathrm{d}s_s\right)v_s, \tag{21}$$

where s_s is the piston area. In order to model the possible damping of the acoustic cavity, the complex frequency $\tilde{\omega}_N$ is replaced by an equivalent real frequency ω_N and an equivalent arbitrary damping coefficient c_N, where $\tilde{\omega}_N = \mathrm{i}\omega_N - c_N/2$. The modal damping ratio ζ_N is related to c_N by $c_N = 2\zeta_N\omega_N$. By rearranging Eq. (18), each acoustic mode amplitude is obtained using

$$\ddot{a}_N + c_N\dot{a}_N + \omega_N^2 a_N = -\frac{c^2}{V\Lambda_N}(Q_N + Q_N^r). \tag{22}$$

The HRs are modeled as piston sources, therefore, the modal forcing term Q_N^r generated by N_r resonators is expressed as a summation

$$Q_N^r = \sum_{h=1}^{N_r}\left(\int_{s_h} \Psi_N^a(\mathbf{r}_h)\,\mathrm{d}s_h\right)\dot{\xi}_h = \sum_{h=1}^{N_r}\phi_{h,N}^a\dot{\xi}_h, \tag{23}$$

where $\dot{\xi}_h$ is the particle velocity at the opening of the hth HR, and s_h is its area. The term $\phi_{h,N}^a$ is one element of the acoustic–HR coupling matrix $\mathbf{\Phi}^a$ given in Eq. (8). Using the resonator's mechanical analog model illustrated in Fig. 2, the HR behavior is described by

$$\rho l_h s_h\ddot{\xi}_h + s_h R_h\dot{\xi}_h + (\rho c^2 s_h^2/V_h)\xi_h = -\int_{s_h} p(\mathbf{r}_h)\,\mathrm{d}s_h, \tag{24}$$

where R_h is the resistance of the HR responsible for its damping level, V_h is the HR volume, and $p(\mathbf{r}_h)$ is the acoustic pressure at the HR opening and $l_h = l + \delta_i$. Using Eq. (14) and (16) in Eq. (24) yields

$$\ddot{\xi}_h + c_h\dot{\xi}_h + \omega_h^2\xi_h = \frac{1}{s_h l_h}\sum_N \dot{a}_N(t)\phi_{h,N}^a(\mathbf{r}_h), \tag{25}$$

where c_h is the HR damping coefficient related to the damping ratio ζ_h by $c_h = 2\zeta_h\omega_h$ and the HR resonant frequency is given by

$$\omega_h = c\sqrt{\frac{s_h}{V_h l_h}}. \tag{26}$$

2.3. Matrix formulation of the system

Using Eqs. (22) and (25) the acoustic cavity–HRs coupled system is put in matrix form as

$$\begin{bmatrix}\mathbf{I}_N & 0\\ 0 & \mathbf{I}_R\end{bmatrix}\begin{Bmatrix}\ddot{\mathbf{a}}\\ \ddot{\boldsymbol{\xi}}\end{Bmatrix} + \begin{bmatrix}\mathbf{C}_N & \mathbf{C}_1\\ \mathbf{C}_2 & \mathbf{C}_R\end{bmatrix}\begin{Bmatrix}\dot{\mathbf{a}}\\ \dot{\boldsymbol{\xi}}\end{Bmatrix} + \begin{bmatrix}\mathbf{\Omega}_N^2 & 0\\ 0 & \mathbf{\Omega}_R^2\end{bmatrix}\begin{Bmatrix}\mathbf{a}\\ \boldsymbol{\xi}\end{Bmatrix} = \begin{Bmatrix}\mathbf{f}_N\\ 0\end{Bmatrix}. \tag{27}$$

$\mathbf{I}_N$ and $\mathbf{I}_R$ are the identity matrix of dimension N, the total number of acoustic modes, and N_r, the total number of HRs, respectively. The vectors $\mathbf{a}$ and $\boldsymbol{\xi}$ group the amplitudes of the velocity potential and the particle velocities at the HR openings. $\mathbf{C}_N$ and $\mathbf{C}_R$ are the diagonal matrices of damping coefficient of the N acoustic modes and of the N_r HRs, respectively. Similarly $\mathbf{\Omega}_N^2$ and $\mathbf{\Omega}_R^2$ are the diagonal matrices of the mode natural frequencies squared and the resonant frequency squared of the HRs. The off diagonal matrices $\mathbf{C}_1$ and $\mathbf{C}_2$ represent the coupling between the HRs

and the cavity. This coupling involves the velocity at the opening of the HRs and the time derivative of the velocity potential mode amplitudes, which, from Eq. (14), are proportional to the acoustic pressure. Using the HR–acoustic coupling matrix $\mathbf{\Phi}^a$ yields

$$\mathbf{C}_1 = \mathbf{\Lambda}_N^{-1}\mathbf{\Phi}^{a\mathrm{T}}c^2/V, \quad \mathbf{C}_2 = -\mathbf{L}_R^{-1}\mathbf{S}_R^{-1}\mathbf{\Phi}^a. \tag{28}$$

$\mathbf{L}_R$, $\mathbf{S}_R$ and $\mathbf{\Lambda}_N$ are the diagonal matrices grouping the effective neck length, the opening area of the HR and the normalization factor of the acoustic mode, respectively. The forcing vector $\mathbf{f}_N$ in Eq. (27) is given by

$$\mathbf{f}_N = -\mathbf{\Lambda}_N^{-1}\mathbf{Q}_N c^2/V. \tag{29}$$

If the acoustic cavity is excited from the inside by an acoustic piston source, the elements of $\mathbf{Q}_N$ are obtained using Eq. (21). When the cavity is excited through the structure, these elements are obtained using Eq. (20). For this particular case, the time-domain structural mode amplitudes v_{N_s} are required. Since the system is only one-way coupled, these amplitudes are independent from the acoustic cavity response and therefore are obtained from the frequency domain model. Using the frequency response of the structural mode amplitude $\mathbf{v}$, impulse response filters are created using the inverse Fourier transform. The convolution of these filters with an external noise source assumed to be a uniformly random signal leads to the time domain structural mode amplitudes. The cylinder scattering of the incident plane wave, the structural coupling with the external pressure field, and the dynamics of the structure are thus included in the forcing vector $\mathbf{f}_N$. Moreover, the effect of a DVA treatment can be taken into account by using the frequency response of the structural mode with a DVA treatment.

The real time adaptation of the HR natural frequencies uses a fourth-order Runge–Kutta technique [16]. For this purpose Eq. (27) is rearranged in state space:

$$\dot{\mathbf{y}}_i = \mathbf{A}_i\mathbf{y}_i + \mathbf{f}_i, \tag{30}$$

where

$$\mathbf{y}_i = \begin{bmatrix} \mathbf{a} \\ \boldsymbol{\xi} \\ \dot{\mathbf{a}} \\ \dot{\boldsymbol{\xi}} \end{bmatrix}, \quad \mathbf{A}_i = \begin{bmatrix} 0 & 0 & \mathbf{I}_N & 0 \\ 0 & 0 & 0 & \mathbf{I}_R \\ -\mathbf{\Omega}_N^2 & 0 & -\mathbf{C}_N & -\mathbf{C}_1 \\ 0 & -\mathbf{\Omega}_R^2 & -\mathbf{C}_2 & -\mathbf{C}_R \end{bmatrix}, \quad \mathbf{f}_i = \begin{bmatrix} 0 \\ 0 \\ \mathbf{f}_N \\ 0 \end{bmatrix}. \tag{31}$$

The state of the system at the following time step $i+1$, which is Δt into the future, is calculated by estimating the gradient of the state vector $\mathbf{y}$ and considering the input force:

$$\mathbf{y}_{i+1} = \mathbf{y}_i + \Delta t\left(\frac{\mathbf{g}_1}{6} + \frac{\mathbf{g}_2}{3} + \frac{\mathbf{g}_3}{3} + \frac{\mathbf{g}_4}{6}\right). \tag{32}$$

The four estimates of the gradient $\mathbf{g}_1$–$\mathbf{g}_4$ are given by

$$\begin{aligned} &\mathbf{g}_1 = \mathbf{A}_i\mathbf{y}_i + \mathbf{f}_i, \quad \mathbf{g}_2 = \mathbf{A}_i(\mathbf{y}_i + 0.5\Delta t\mathbf{g}_1) + \mathbf{f}_{i+1/2}, \\ &\mathbf{g}_3 = \mathbf{A}_i(\mathbf{y}_i + 0.5\Delta t\mathbf{g}_2) + \mathbf{f}_{i+1/2}, \quad \mathbf{g}_4 = \mathbf{A}_i(\mathbf{y}_i + \Delta t\mathbf{g}_3) + \mathbf{f}_{i+1}. \end{aligned} \tag{33}$$

At each time step, the matrix $\mathbf{A}_i$ can be modified as the natural frequency of the HRs $\mathbf{\Omega}_R$ are adjusted to minimized some cost function.

3. The dot-product method

As a preliminary study for the new adaptive resonator concept presented in this paper, a comparison between local and global strategies for the control of a set of modes was undertaken by Johnson and Estève [12]. The idea is to investigate the interaction of multiple single dof systems with a continuous system described by a set of modes. The shape of different local cost functions due to tuning of these single dof systems is studied and compared to a global cost function. In Ref. [12] the concrete example of a vibrating structure on to which multiple vibration absorbers are attached is adopted to describe the different cost functions. The acoustic analog of this mechanical system corresponds to an acoustic cavity coupled to multiple HRs. The pressure mode amplitudes of the cavity are then equivalent to the velocity mode amplitudes of the structure, the pressure at the opening of a HR is equivalent the base velocity of a vibration absorber, and finally the pressure inside a HR is equivalent to the velocity of the absorber mass. In this analysis, Johnson and Estève [12] show that the dot-product method is the only local cost functions of the set that converge very close to a global solution for a multi-mode single absorber case. This conclusion remains valid for the multi-mode multi-absorber case. Therefore, the dot-product method is adopted here to tune multiple HRs. The mechanisms of this particular tuning law are presented and analyzed in detailed in the next section for both single frequency and broadband excitation.

3.1. Single frequency excitation

For a single dof vibration absorber, the tuning is achieved when the motion of the structure and the absorber mass are in quadrature. The dot-product method is a tuning law developed for adaptive vibration absorbers in single frequency control applications. It works by evaluating the integral over a period of the excitation frequency of the product between the velocity amplitudes of the absorber mass $\dot{x}_a(t)$ and the host structure $\dot{x}_s(t)$. Taking the dot-product of the two discrete time signals approximates this integral. By expressing for single-frequency excitation these time signals as $\dot{x}_s(t) = \dot{X}_s \cos(\omega t)$ and $\dot{x}_a(t) = \dot{X}_a \cos(\omega t - \phi)$, Long et al. [10] showed that the dot-product is proportional to a cosine function of the phase angle between the host structure and the absorber mass as

$$\frac{1}{T}\int_{T/2}^{T/2} \dot{x}_s(t)\dot{x}_a(t) = \frac{|\dot{X}_s||\dot{X}_a|}{2}\cos(\phi). \tag{34}$$

When the two signals are in quadrature, the absorber is tuned and, assuming a lightly damped absorber, the dot-product is approximately zero. As a consequence, the sign of the product can be used to tune the absorber to the excitation frequency. When the absorber is over-tuned, the two signals are almost in phase and the dot-product is positive. When the absorber is under-tuned, the two signals are mostly out of phase and the dot-product becomes negative. The dot-product also gives information on the magnitude of the tuning error. Using the acoustic analog, this tuning algorithm is applied to a tunable HR by evaluating the dot-product between the pressure amplitudes inside the HR, p_{int}, and at its opening, p_{ext}. In this particular case, the dot-product, x_p,

is therefore given by

$$x_p = \frac{1}{T}\int_{T/2}^{T/2} p_{\text{int}}(t)p_{\text{ext}}(t)\,\mathrm{d}t. \tag{35}$$

3.2. Broadband excitation

Under broadband excitation, the product of the two signals is integrated over an arbitrary period T. This integral provides an estimate at $\tau = 0$ of the cross-correlation function $X_{p_{\text{int}},p_{\text{ext}}}(\tau)$ between p_{int} and p_{ext} which is expressed as

$$X_{p_{\text{int}},p_{\text{ext}}}(\tau) = \int_{-\infty}^{+\infty} p_{\text{int}}(t)p_{\text{ext}}(t-\tau)\,\mathrm{d}t. \tag{36}$$

It can be seen that by setting $\tau = 0$ and integrating over the finite period T (from $-T/2$ to $T/2$), Eq. (36) reduces to Eq. (35) but for the $1/T$ factor. The longer the period T is, the more accurate the correlation estimation becomes. The cross-correlation $X_{p_{\text{int}},p_{\text{ext}}}(\tau)$ can also be expressed as the inverse Fourier transform of the cross-spectrum $G(\omega)$ of the two signals:

$$X_{p_{\text{int}},p_{\text{ext}}}(\tau) = \int_{-\infty}^{+\infty} G_{p_{\text{int}},p_{\text{ext}}}(\omega)\mathrm{e}^{\mathrm{j}\omega\tau}\,\mathrm{d}\omega. \tag{37}$$

Using the even and odd properties of the real and imaginary part of the cross-spectrum, the dot-product reduces to

$$X_{p_{\text{int}},p_{\text{ext}}}(\tau = 0) = \int_{0}^{+\infty} \mathrm{Re}(G_{p_{\text{int}},p_{\text{ext}}}(\omega))\,\mathrm{d}\omega. \tag{38}$$

For frequencies well below the first mode of the HR cavity, the HR internal pressure p_{int} is uniform. As long as the frequency band of control remains below the first mode of the HR cavity, the HR internal pressure p_{int} is proportional to the volume velocity at its opening u [17]:

$$p_{\text{int}}(\omega) = \frac{\rho c^2}{\mathrm{i}\omega V_h}u(\omega). \tag{39}$$

Using the single dof mechanical analog of Fig. 2, the HR admittance Y_h relating the HR volume velocity to the impinging pressure at its opening, p_{ext} is expressed as

$$u(\omega) = Y_h(\omega)p_{\text{ext}}(\omega) = \frac{\mathrm{i}\omega\omega_h^2 V_h}{\rho c^2[(\omega_h^2-\omega^2) - 2\mathrm{i}\varsigma_h\omega\omega_h]}p_{\text{ext}}(\omega). \tag{40}$$

Substituting Eq. (40) in Eq. (39), the internal pressure is expressed as a function of the external pressure

$$p_{\text{int}}(\omega) = \frac{\omega_h^2}{[(\omega_h^2-\omega^2) - 2\mathrm{i}\varsigma_h\omega\omega_h]}p_{\text{ext}}(\omega). \tag{41}$$

The cross-spectrum of the two pressure signals then reduces to

$$G_{p_{\text{int}}p_{\text{ext}}} = p_{\text{int}}(\omega)p^*_{\text{ext}}(\omega) = \frac{\omega_h^2}{[(\omega_h^2 - \omega^2) - 2\text{i}\varsigma_h\omega\omega_h]}|p_{\text{ext}}(\omega)|^2. \tag{42}$$

Eq. (42) shows that the real part of the cross-spectrum is positive below the HR tuning frequency and negative above. Driving the dot-product given in Eq. (38) to zero tunes the HR such that an equal amount of the real part of the cross-spectrum lies above and below its natural frequency. Consequently, HRs are attracted to peaks in the spectrum of p_{ext} where most of the acoustic energy is concentrated. Placed in a resonant environment, the HRs tune to the lightly damped modes of the cavity where they are the most effective in adding damping and thus have a global effect on the noise level as illustrated in Fig. 3. To be effective, the HR needs to be positioned at the antinodes of acoustic modes. Since the dot-product evaluation is local, the acoustic modes with nodes at the HR position are not captured in the p_{ext} spectrum and so the HR will not tune to these uncontrollable modes. Therefore, the local tuning law, ensure the tuning to occur at frequencies where the HR are the most effective in reducing the noise. However, if peaks in the spectrum of p_{ext} correspond to lightly structural resonances, the HR will tune to these peaks without damping them significantly. These structural resonances can be attenuated efficiently with DVAs to avoid a non-optimal use of HRs. Another property of this method is the high-frequency filtering of the broadband excitation due to the natural dynamics of the HR. Indeed, as seen in Eq. (42), the displacement–force admittance of the HR provides a -12 dB per octave filter above the tuning frequency. Excited with a constant volume velocity source, the acoustic resonances of the cavity (p_{ext}) present a velocity–force admittance behavior with symmetric slopes of 6 and –6 dB per octave before and after the natural frequency. Combining these two types of responses with Eq. (42) leads to band-passed filter properties for the cross-spectrum. However, if the cavity is excited by a constant volume acceleration source, the acoustic resonances (p_{ext}) present the same displacement–force admittance behavior as the resonator. Consequently, the cross-spectrum

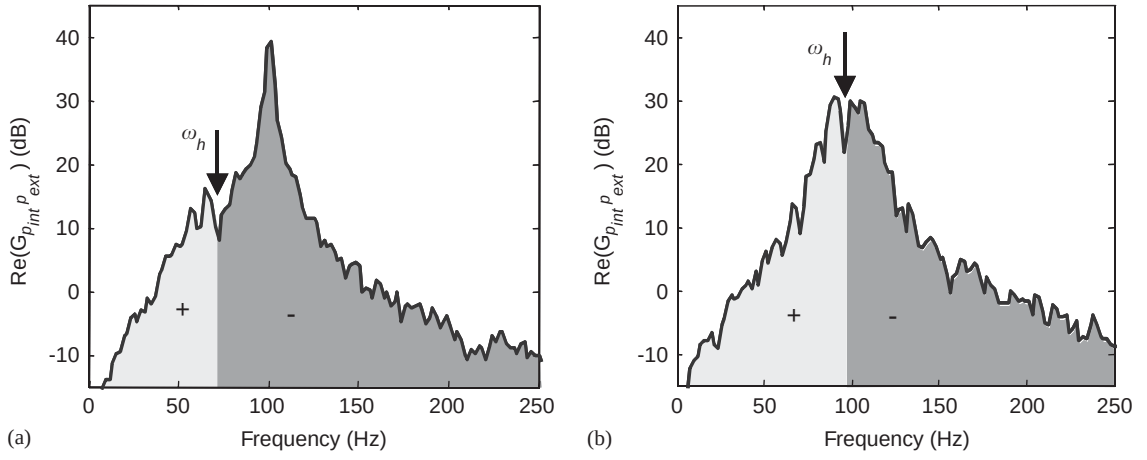

Fig. 3. Real part of the cross-spectrum of (a) an under-tuned HR and (b) tuned HR with respect to a single resonance at 100 Hz.

behaves as a sixth-order low-pass filter. This may cause an under tuning of the HR by biasing the dot-product to the low frequencies. Therefore, when the cavity is excited with a constant acceleration source such as a speaker, the dot-product can be evaluated using the derivative of the pressure signals. The resulting cross-spectrum presents band-passed filter properties, which ensure a more accurate tuning. In the model, the pressures inside the HR and at its opening are expressed as

$$p_{\text{int}} = \rho c^2 / V_h \xi_h \quad (i = 1, \ldots, n), \quad p_{\text{ext}} = -\rho \sum_N \phi^a_{h,N} \dot{a}_N \quad (i = 1, \ldots, n), \tag{43}$$

where n is the number of time steps defining the period T. In order to limit its absolute value by unity, the dot-product, x_p, is also normalized:

$$x_p = \frac{p_{\text{int}} \cdot p_{\text{ext}}}{\sqrt{(p_{\text{int}} \cdot p_{\text{int}})(p_{\text{ext}} \cdot p_{\text{ext}})}}. \tag{44}$$

4. Numerical simulation

The following numerical simulations correspond to a 2.8 m long 2.5 m diameter composite cylinder built by Boeing and used for the experiments presented in Section 5. The shell theory and numerical values used to obtain the structural natural frequency of the cylinder are identical as in Ref. [1]. For the real-time adaptation simulation, the length of the HR neck is chosen to vary the HR tuning frequency.

4.1. Single mode forced by an internal source

In this section, the acoustic forcing is provided by a piston source inside the cavity; therefore, because the model is only one-way coupled, the dynamics of the structure do not intervene in the computation. The source modeled as a random signal is positioned at the bottom of the cylinder (axial position $z = 0$, radial position $r = 1.23$, and circumferential position $\theta = \pi$). Only the first mode of the cavity with a natural frequency of 61.7 Hz and a damping ratio of 1% is taken into account. Three identical HRs are positioned at the boundary (i.e. $r = 1.23$), at the bottom of the cylinder ($z = 0$) and are evenly distributed around the circumference ($\theta = 0, 2\pi/3, 4\pi/3$). The total volume of the HRs represents 0.6% of the cavity volume. The HR optimal damping ratio is set to 5.2% [1]. The initial length of the necks are 12, 20 and 15 cm, which provide initial tuning frequencies of 66.7, 55.1 and 62.0 Hz, respectively. This configuration represents the over-tuned, under-tuned and tuned cases for the HRs. Using the Runge–Kutta model with a time step of 1 ms, the necks of HRs are sequentially adapted by 2.5 mm increments according to the value of the dot-product evaluated over a period of 0.5 s. This sequential tuning strategy was adopted to be consistent with the experiments presented in Section 5. Indeed, the experiments were performed using a sequential controller. The use of a simultaneous controller to optimize the adaptation speed will be investigated in future work. In this simulation, the HRs stop tuning when the absolute value of the normalized dot-product drops below 0.01. Fig. 4 shows the evolution of the dot-product and the tuning frequency for the three HRs as a function of time. As expected, the

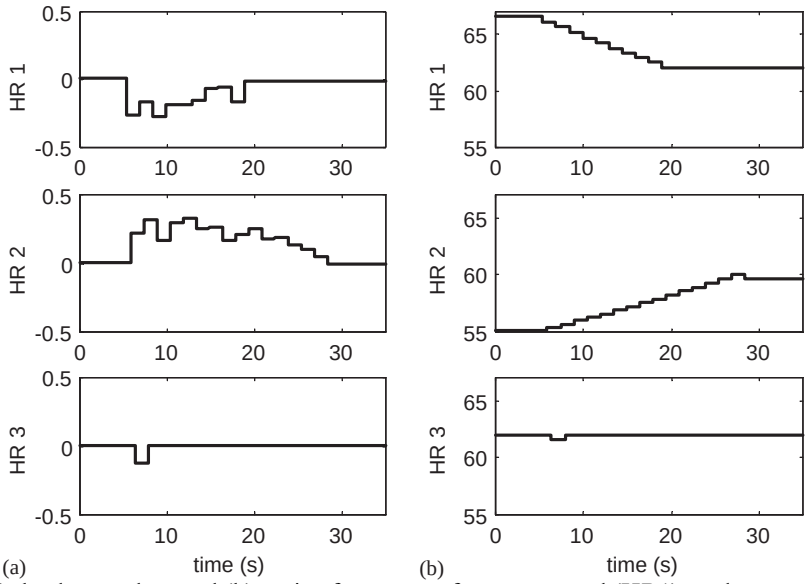

Fig. 4. Change in (a) the dot-product and (b) tuning frequency of an over-tuned (HR1), under-tuned (HR2), and tuned (HR3) resonator as a function of time.

first HR drops its natural frequency down to 62.1 Hz, the second raises it to 59.6 Hz and the third one maintains it at 62.0 Hz. The adaptation time for the three HRs is less than 25 s (during the first 5 s, HRs are inactive).

4.2. *Multi-mode forced by an external plane wave*

In this section, the acoustic cavity is forced through the structure by an incident plane wave ($\alpha_i = 70^\circ$). Fig. 5 shows the kinetic and acoustic energy obtained with the one-way coupled frequency domain model with and without the DVA treatment. The simulation includes 36 structural modes and 17 acoustic modes with natural frequencies below 200 Hz. The DVA treatment, representing 2% of the cylinder mass, consists of a ring of 13 absorbers distributed evenly around the circumference and placed halfway up the cylinder wall. The damping ratio of the structural mode is set to 1% whereas the damping ratio of the DVAs is set to its optimal value of 10% [1]. The DVAs target the most excited structural mode at 112.5 Hz, which also couples best to the acoustic cavity. Once this structural resonance is damped by the DVAs, the remaining peaks in the acoustic energy spectrum correspond to the acoustic modes of the cavity and thus can be damped by HRs. Without DVAs, a HR could tune to any structural peaks in the acoustic spectrum even if it cannot damp them efficiently.

The HR treatment consists of two rings of five resonators placed at the bottom and halfway up the cylinder walls. As for the DVAs, the five HRs are evenly distributed around the circumference. The total volume of the HR treatment represents 4% of the cavity volume, and their damping ratio is set to 9%. The time-domain velocity amplitudes of the structural modes with the DVA treatment are substituted in the Runge–Kutta model. The time step is set to 0.5 ms. The adaptation is continued until all the HRs are considered tuned, when the absolute value of their

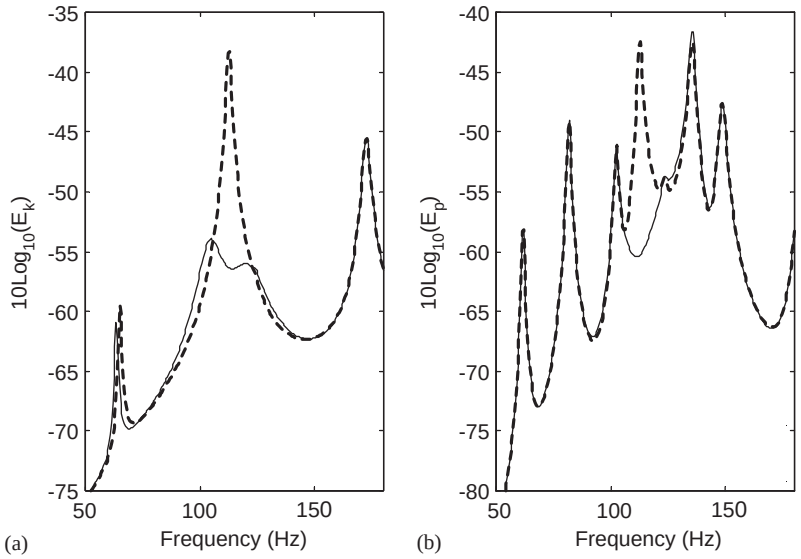

Fig. 5. (a) Structural kinetic energy and (b) acoustic potential energy of the cylinder with (solid line) and without DVA treatment (dash line) for the one-way coupled model.

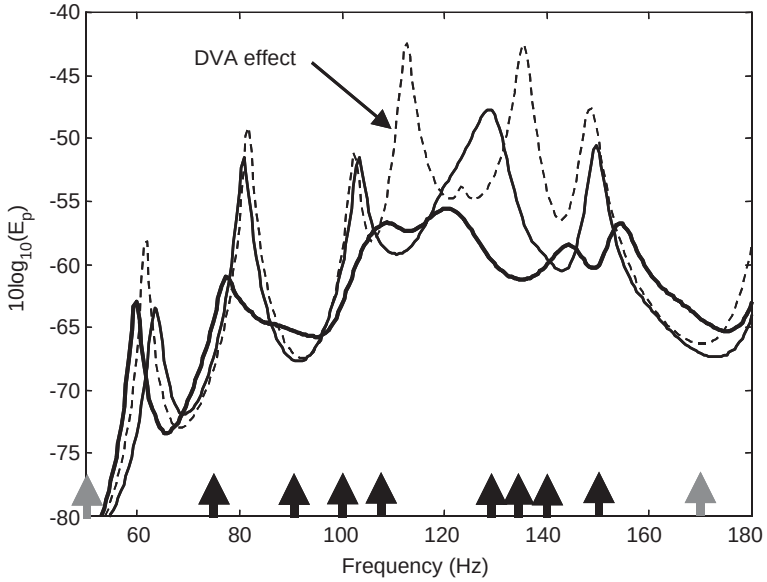

Fig. 6. Acoustic potential energy before (faint line) and after adaptation (solid line) compared to the bare case (dash line).

normalized dot-product is less than 0.01. In this particular case, the adaptation lasts around 2 min (around 12 s per HR). Fig. 6 shows the acoustic potential energy for the bare cylinder and the cylinder treated with HRs and DVAs before and after the adaptation. The initial tuning frequency of the bottom and middle ring illustrated by the gray arrows in Fig. 6 are 50 and 170 Hz,

respectively. The final tuning frequencies (black arrows) are for the bottom ring [107.2,89.6,109.5,101.1,76.5] Hz and for the middle ring [148.1,146.3 136.9,136.1,130.1] Hz.

Initially tuned to 50 and 170 Hz, the acoustic attenuation from 40 to 160 Hz is 3.4 dB, where 1 dB is due to the DVAs. Even though they are not tuned, the HRs can still absorb some energy of the neighboring peaks because of their high damping level, which broadens their frequency range of action. However, once the adaptation is over the acoustic attenuation from 40 to 160 Hz increases up to 7.5 dB. This performance is similar to 7.7 dB obtained in Ref. [1] where five rings of five HRs each, representing 6% of the cavity volume, were tuned to the five dominant acoustic resonances between 40 and 160 Hz. These simulations demonstrate that, as long as the structure modes, which strongly couple to the acoustic cavity, are damped with a DVA treatment, the dot-product method converges to a near-optimal solution.

5. Experimental results

This section describes the experiments conducted on the Boeing composite cylinder (see Fig. 11). The key objective of these experiments is to test how the HRs adapt to multiple resonances using the dot-product method. The cylinder acoustic cavity is therefore, excited using and internal speaker and not through the structure. These conditions, allow concentrating the effort on the design of the adaptive HRs and the control system, since no structural resonances are well excited by the internal speaker. Therefore, DVAs, which have been tested before and proven successful [3] are not required in these experiments.

5.1. Adaptive HR prototype

According to Eq. (26), changing the resonant frequency of a HR can be achieved by modifying the volume, the opening area or the neck length. De Bedout et al. [6] built a tunable resonator with a variable volume. This solution probably allows the widest tuning range and ensures the natural frequency to vary as the square root of the volume. However, the HR efficiency is proportional to its volume [15], and therefore this device has reduced efficiency when tuned above its lowest frequency. In addition, the weight of the machinery required to change a sealed volume renders such a device unsuited for aerospace applications.

Several designs of tunable HR with fixed volume were investigated. The best compromise between tuning range and compactness is obtained for a variable opening HR as shown in Fig. 7. The resonator cavity is made of a cardboard tube of 12.7 cm in diameter and enclosed with plastic end-caps. On the top end-cap, an iris diaphragm provides the variable opening whose diameter ranges from 9 to 58 mm. The length of the tube (56 cm) was chosen to obtain a tuning range including the first three acoustic mode of the cylinder at 63, 82, and 103 Hz. Using a pulley mechanism, a lightweight (28 g) small step motor is used to rotate the iris control arm as shown in Fig. 8. This mechanism represented an easy, off the shelf and inexpensive solution. The adaptive HR is equipped with two microphones; one placed in front of the opening, and the other flush mounted to the back end cap to monitor the internal pressure. These two microphones provide the two signals needed to evaluate the dot-product. Exciting the resonator with a speaker driven with white noise, the transfer function between the two microphones are measured and used to

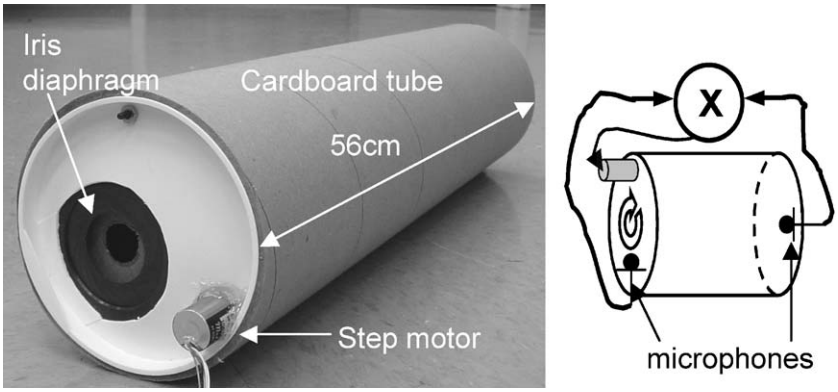

Fig. 7. Adaptive HR prototype.

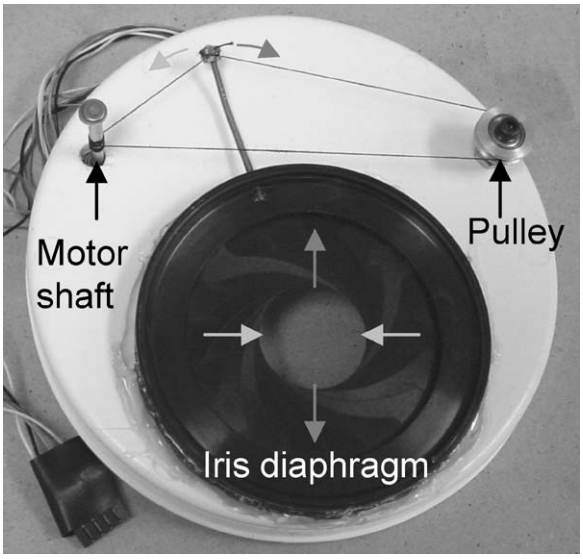

Fig. 8. Motorized iris diaphragm mechanism.

evaluate the natural frequency and damping ratio for different opening diameters. Because of the 90° minimum step angle of the motor, only 30 different diameters can be obtained. The resulting frequency resolution of approximately 2 Hz is sufficient for this particular application, which requires damped HRs. The resulting tuning curve is shown in Fig. 9. The good agreement between the measured and the predicted natural frequency is obtained using a different neck length for each opening diameter in Eq. (26). Indeed, as the leaves of the iris fold to open, the physical neck increase from a minimum of 1 mm to a maximum of 10 mm due to the additional frame and end-cap thickness. In Fig. 9 it can also be seen that the damping of the resonator varies significantly with the tuning frequency. Created by viscous losses, the damping increase nonlinearly as the HR opening is reduced. A fairly constant level of damping through out the frequency range is

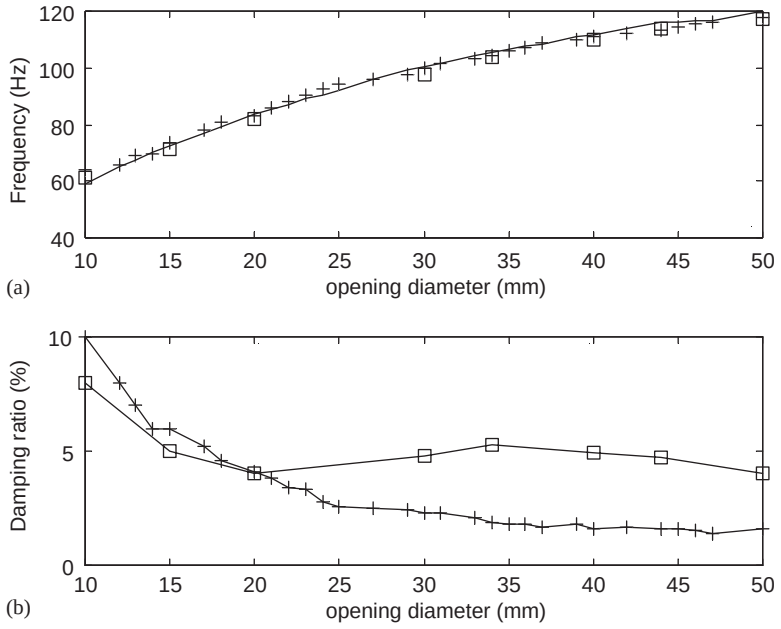

Fig. 9. (a) HR natural frequency and (b) damping ratio for different opening diameters. Solid line, predicted; +, measured; □, measured with screen.

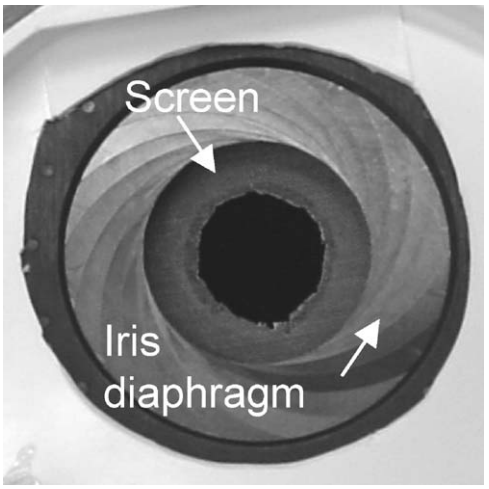

Fig. 10. Iris diaphragm with wire mesh screen for constant damping.

preferable to ensure the optimal performance of the HR. As a solution, a wire mesh screen is placed over the opening to increase the damping levels, for diameters greater than 20 mm. To avoid a further increase of damping, already too high for smaller diameters, a 20 mm diameter disk is cut out of the center of the screen as shown in Fig. 10. The measured natural frequency and damping ratio with this screen is also plotted in Fig. 9. The resonance of the HR is not affected by

the presence of the screen. In addition, the screen ensures a more constant and favorable damping level of 5% throughout the tuning range except for the lowest three frequencies.

5.2. Control system

The main advantage of the dot-product method is its possible implementation using analog circuitry, which reduces the controller complexity, cost, and weight. Indeed, the analog signals of the two microphones can be summed and then low-pass filtered yielding a positive or negative continuous voltage that can then control the rotation of a standard DC motor. To avoid tuning the HR outside of its functional range band-pass filtering of the two microphone signals around this range would be sufficient. This simple scheme permits the integration of sensor, actuator and controller into one generic device.

However, in this work, a digital centralized controller was developed to mimic the behavior of multiple independent analog controllers. This centralized controller was more suitable to observe the tuning mechanisms of several HRs simultaneously. This control system uses a Labview ® interface and is composed of two parts. The first part is the data acquisition system used to acquire the time signals of the microphones. The second is the stepper motor driver, which uses the parallel port of the computer and an electronic circuit composed of decoders and transistor arrays. A 5 and 28 V power supply is required for the electronics and the stepper motor, respectively. This system allows the control of up to eight motors sequentially. Given the initial diameter of the opening, the system tracks the iris variations and stops the motor whenever the physical limits of the opening are reached.

5.3. Experimental setup

Eight adaptive HRs identical to the one in Fig. 7 each equipped with two microphones were built. A speaker was placed at the bottom of the cylinder as seen in Fig. 11 and driven with 40–200 Hz band passed white noise to excite the acoustic cavity. Three rings of five microphones positioned at 48, 137, 233 cm from the bottom and 33 cm from the wall were used to obtain a spatial average of the acoustic pressure inside the cylinder. A last microphone was placed inside the disturbance speaker cabinet in order to estimate the volume velocity (VV) of the source [17]. The auto-spectra of all the microphones and their cross-spectrum with respect to the microphone placed inside the speaker cabinet can be acquired simultaneously. The total volume of the resonator represents only 0.4% of the cylinder's cavity. As a consequence, to obtain the best efficiency, the eight HRs are positioned as illustrated in Fig. 11 with their opening towards the cylinder wall. In this configuration, the HRs are placed at antinodes of the first three acoustic modes which orient with respect to the disturbance speaker.

5.4. Results

The microphone signals are first acquired when the HRs are inside the cylinder with tape over their opening which renders them inactive. This configuration is called "bare" since it is equivalent to the empty cylinder apart from the small volume taken by the HR. The tape is then removed from the HR throats and the opening diameters are set to some initial value. The data is acquired

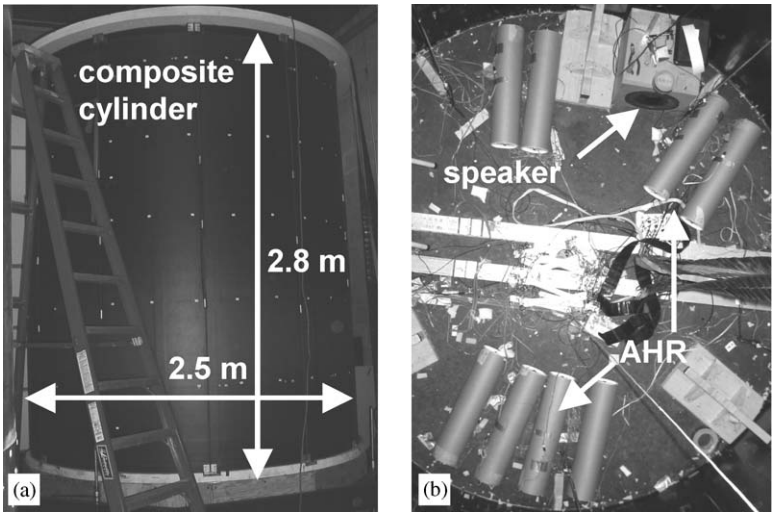

Fig. 11. (a) Composite cylinder and (b) AHRs placed inside (top view) the cylinder.

in this configuration, which is called ''before adaptation''. The control system is turned on, and using the time signal of the HR microphones the adaptation begins. When the opening diameter of each HR has converged, the control is turned off and all the sensor signals are acquired to evaluate this ''after adaptation'' configuration.

The objective of this first experiment is to verify the tuning algorithm on a single mode. The HR microphones signals are therefore digitally band-pass filtered around the third mode of the acoustic cavity at 103 Hz. The cut-on frequencies of the sixth-order Butterworth filters used were 95 and 115 Hz. As explained in Section 3.2 the time derivative of the microphone signals are used to compute the dot-product. To control the sensitivity of the tuning algorithm to noise introduced by the signal differentiation, the dot-product threshold below which the HRs are considered tuned is set to 0.05. The opening diameters of the HR are set initially to 12 mm and the eight HRs are adapted sequentially. With a sampling frequency of 1024 Hz, the dot-product is evaluated over 1 s using 1024 points. The adaptation process is carried on for about 5 min, each iteration lasting about 1 s. Fig. 12 plots the opening diameter of the eight HRs at each iteration. After convergence, the HRs show some changes in the opening diameter corresponding to small tuning frequency variations (see Fig. 9). These perturbations can be associated to the changes in the disturbance due to the stochastic nature of the input. The effects of these small variations on the performance were found to be negligible. Table 1 lists the corresponding initial and final tuning frequencies obtained from the transfer function between the two microphones at each HR. As an example, the transfer function of two HRs before and after adaptation is plotted in Fig. 13 showing the shift in their natural frequency. Note that these transfer functions are obtained as a ratio of the cross spectrum of the two microphones with respect to the microphone placed in the speaker cabinet, and the spike around 90 Hz comes from the ratio of a zero in both cross spectra. To further illustrate the convergence of the HRs toward the 104 Hz-targeted resonance, Fig. 14 plots for two HRs the real part of the normalized cross-spectrum after band-passed filtering. Initially under-tuned, the arithmetic area under the gray curve corresponding to the dot-product value x_p is negative. Once tuned, the positive and negative area under the black curve balances out

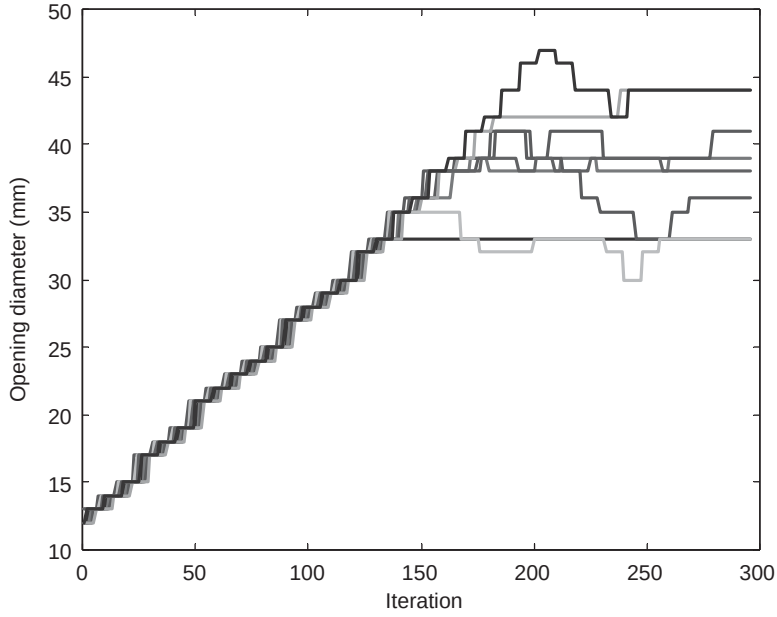

Fig. 12. Evolution of the opening diameter for the eight HRs for the single-mode experiment.

Table 1
Tuning frequency of the eight HRs before and after the single-mode adaptation

	Tuning frequency (Hz)	
HR #	Before adaptation	After adaptation
1	72	105.5
2	69	105
3	66	104.5
4	67	105
5	69	108
6	70	101.5
7	67	101
8	67	106

yielding a dot-product value close to zero. The transfer functions between 14 monitoring microphones and the microphone placed inside the speaker cabinet are used to get the average sound pressure level inside the cylinder. Fig. 15 compares the acoustic response of the cavity for the bare, before and after adaptation cases. Even though the HRs are initially detuned around 70 Hz, they add some damping to the three acoustic peaks compare to the bare case. Once tuned, the HRs provide a 6.5 dB attenuation in the 95–115 Hz bandwidth of control.

The objective of this second experiment is to verify that the tuning algorithm would still performs as expected in a multi-mode case. Although the HRs can tune to any of the first three acoustic resonances of the cylinder, the bandwidth of control is set around the last two. The

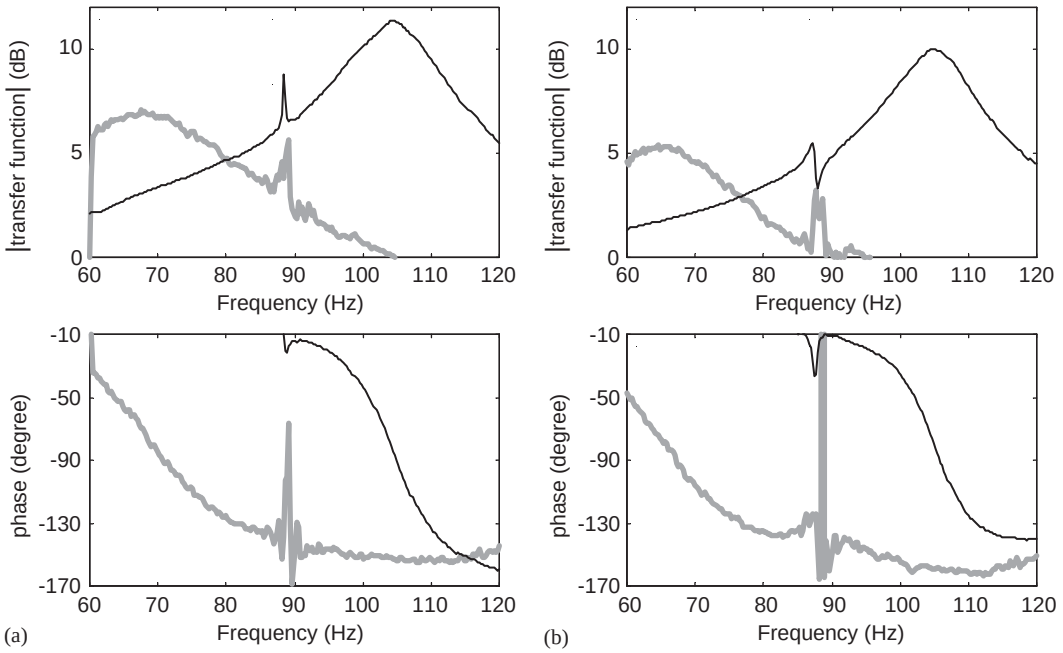

Fig. 13. Magnitude and phase of the transfer function of (a) HR #2 and (b) HR #8 for the single-mode experiment before adaptation (gray line) and after adaptation (black line).

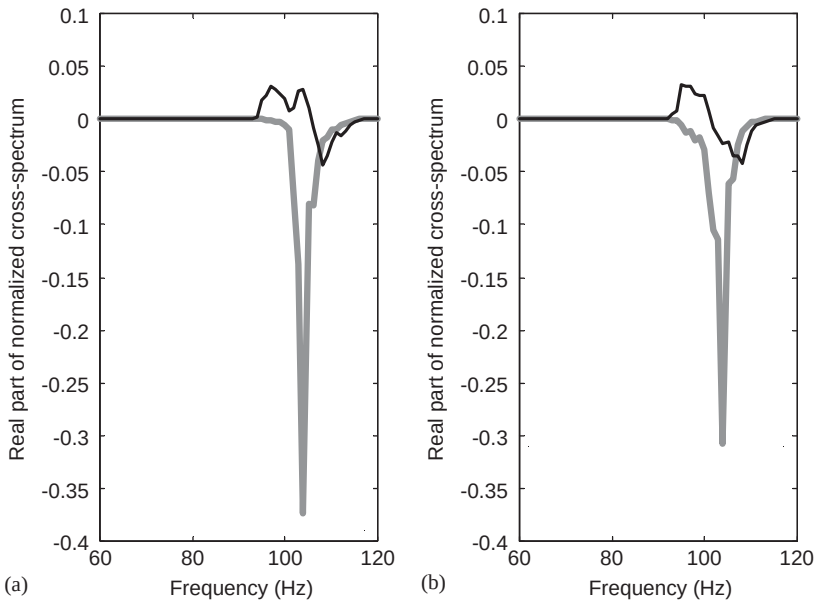

Fig. 14. Normalized cross-spectrum of (a) HR #4 and (b) HR #6 before adaptation (gray line) and after adaptation (black line) for the single-mode experiment.

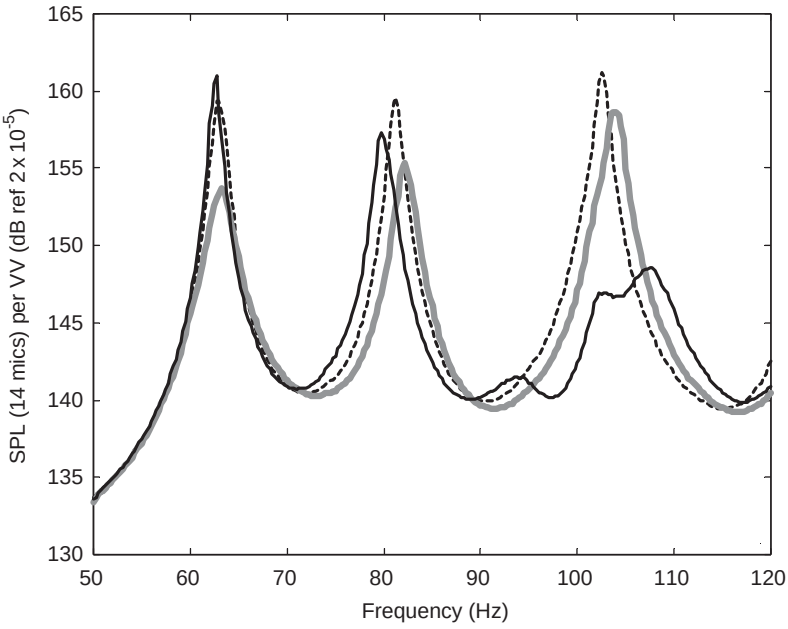

Fig. 15. Measured acoustic response of the cavity before (gray line) and after the adaptation (black line) compared to the bare response (dash line) for the single-mode experiment.

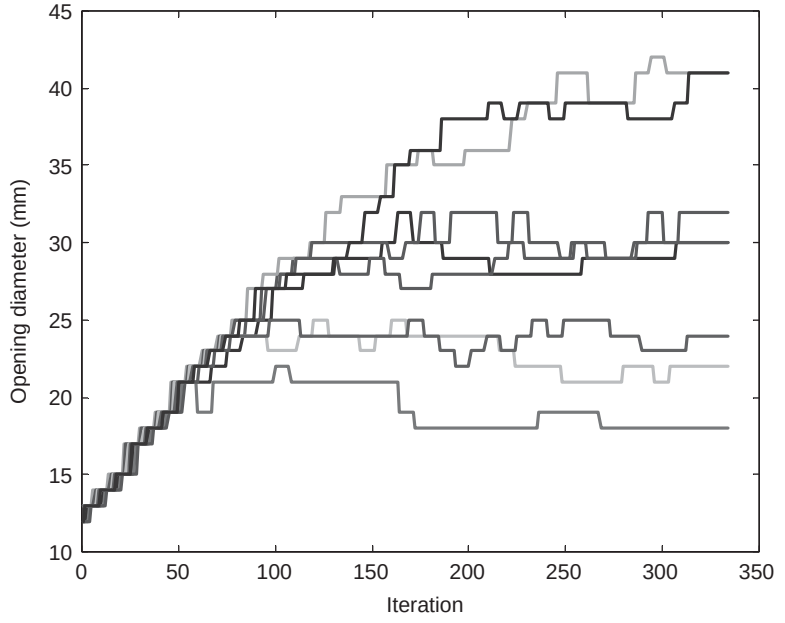

Fig. 16. Evolution of the opening diameter for the eight HRs for the multi-mode experiment.

unavoidable high damping level of the HR near 64 Hz and the sharing of the already small 0.4% volume ratio on three different modes will not lead to significant attenuation of the three peaks. The digital filter cut-on frequencies for the HR signals are set to 75 and 115 Hz, and the

adaptation is carried on using the same procedure as with the single-mode experiment. Fig. 16 illustrates the evolution of the opening diameter and Table 2 lists the corresponding initial and final HR tuning frequencies. As observed in the simulation, the HRs spread their natural frequencies across the bandwidth of control. Fig. 17 shows the real part of the normalized cross-spectrum for HR #2 tuned to the second mode and HR #4 tuned to the third. In both cases the dot-product initially negative converges towards zero. The acoustic response of the cavity plotted in Fig. 18 demonstrates the global effect of the tuning algorithm as both targeted peaks are reduced by 6 and 8 dB compared to before the adaptation. The resulting overall attenuation in the 75–115 Hz bandwidth of control is 4.2 dB.

Table 2
Tuning frequency of the eight HRs before and after the multi-mode adaptation

	Tuning frequency (Hz)	
HR #	Before adaptation	After adaptation
1	72	102.5
2	69	81
3	66	90
4	67	102
5	69	97
6	70	88
7	67	86
8	67	103

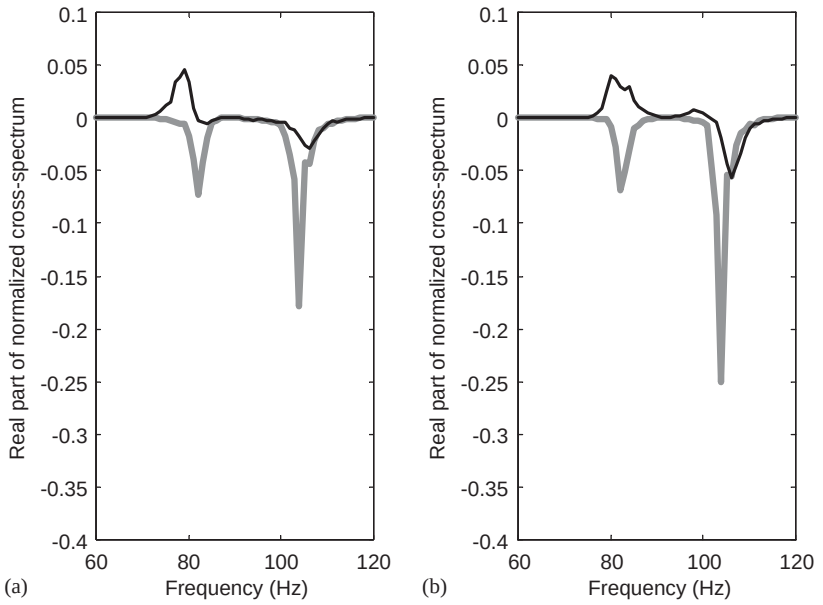

Fig. 17. Normalized cross-spectrum of (a) HR #2 and (b) HR #4 before (gray line) and after the adaptation (black line) for the multi-mode experiment.

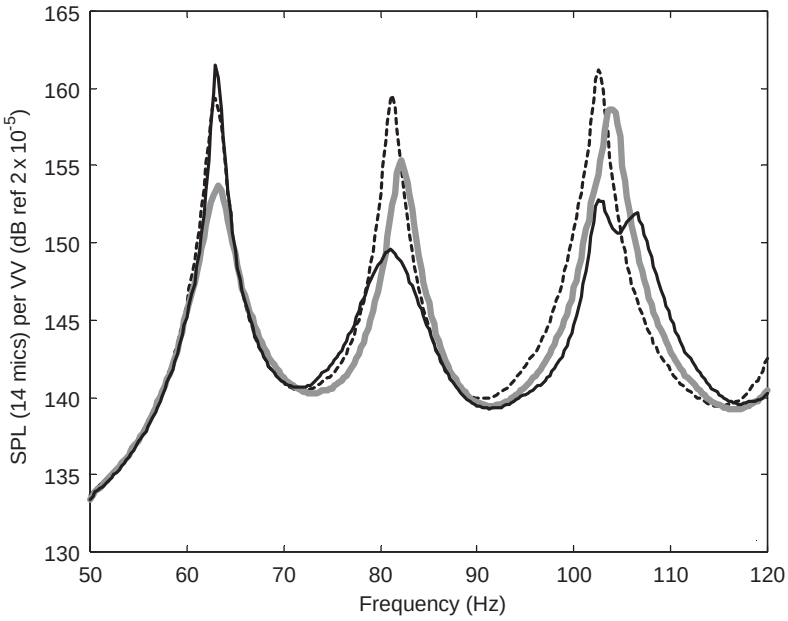

Fig. 18. Measured acoustic response before (gray line) and after adaptation (black line) compared with the bare response (dash line) for the multi-mode experiment.

6. Conclusions

For this study, both a time and a frequency domain model of a composite cylinder excited by an external plane wave have been developed. Using a state-space approach and a fourth Runge–Kutta technique, the model couples together the structure, the acoustic cavity and two types of noise reduction devices: DVAs (applied to the structure) and HRs (applied to the acoustic cavity). The dot-product method commonly used to tune absorber to single frequency excitation was applied in a new fashion to HRs for broadband frequency excitation. Under this tuning law, the HRs can track changes in the natural frequencies of the acoustic cavity, caused by varying payload fills, and hence maintain their performance. This strategy presents several advantages: it uses information that is local to each devices and thus is more practical than global strategies, and it can be implemented using simple analog circuitry which allows each device to be manufactured as an autonomous generic device.

The numerical simulations have first demonstrated that the dot-product method allows HRs to adapt to the natural frequency of a single acoustic mode of the cavity excited by an internal source. When the excitation is produced by an external plane wave, simulations using 17 acoustic modes showed that the dot-product method tunes the HRs to a near-optimum solution, 7.5 dB noise reduction in the 40–160 Hz band. However, this requires the structural resonances, which appear in the acoustic spectrum, to be damped with a DVA treatment.

A prototype of adaptive HR with variable opening was built and characterized. A centralized controller mimicking the behavior of multiple independent local controllers was developed in order to track and observe the tuning mechanisms of up to eight HRs simultaneously. The experiments carried on a large composite cylinder with eight adaptive resonators validated the

simulations and demonstrated the ability of the dot-product method to tune resonators to near-optimal solution over a frequency band including multiple resonances.

Acknowledgement

The support of the Boeing Company is gratefully acknowledged.

References

[1] S.J. Estève, M.E. Johnson, Reduction of sound transmitted into a composite cylinder using distributed vibration absorbers and Helmholtz resonators, *Journal of the Acoustical Society of America* 112 (6) (2002) 2040–2048.
[2] S.J. Estève, M.E. Johnson, Control of the noise transmitted into a cylinder using optimally damped Helmholtz resonators and distributed vibration absorbers, *Proceedings of the Ninth International Congress on Sound and Vibration*, Orlando, FL, July 2002, Paper 522.
[3] H. Osman, M.E. Johnson, C.R. Fuller, S.J. Estève, P. Marcotte, Application of damped Helmholtz resonators and distributed vibration absorbers for the control of noise transmission into a cylinder, *Proceedings of the Ninth International Congress on Sound and Vibration*, Orlando, FL, July 2002, Paper 509.
[4] R.J. Bernhard, The state of the art of active–passive noise control, *Proceedings of Noise-Con 94*, Ft. Lauderdale, FL, 1994.
[5] J.S. Lamancusa, An actively tuned, passive muffler system for engine silencing, *Proceedings of Noise-Con 87*, The Pennsylvania State University, PA, 1987.
[6] J.M. de Bedout, M.A. Franchek, R.J. Bernhard, L. Mongeau, Adaptive-passive noise control with self-tuning Helmholtz resonators, *Journal of Sound and Vibration* 202 (1) (1995) 109–123.
[7] T.M. Kostek, M.A. Franchek, Hybrid noise control in ducts, *Journal of Sound and Vibration* 237 (1) (2000) 81–100.
[8] K. Nagaya, Y. Hano, A. Suda, Silencer consisting of a two stage Helmholtz resonator with auto tuning control, *Journal of the Acoustical Society of America* 110 (1) (2001) 289–295.
[9] J. Dayou, M.J. Brennan, Global control of structural vibration using multiple-tuned tunable vibration neutralizers, *Journal of Sound and Vibration* 258 (2) (2002) 345–357.
[10] T. Long, M.J. Brennan, S.J. Elliot, Design of smart machinery installations to reduce transmitted vibrations by adaptive modifications of internal forces, *Proceedings of the Institution of Mechanical Engineers* 212 (Part I) (1998) 215–228.
[11] M.R.F. Kidner, M.J. Brennan, Varying the stiffness of a beam-like neutralizer under fuzzy logic control, *Journal of Vibration and Acoustics* 124 (2002) 90–99.
[12] M.E. Johnson, S.J. Estève, Comparison of local and global adaptive strategies for the control of broadband noise in an enclosure using adaptive Helmholtz resonators, *Proceedings of the Active 2002 Conference*, Institute of Sound and Vibration Research, University of Southampton, UK, July 2002.
[13] L.E. Kinsler, A.R. Frey, A.B. Coppens, J.V. Sanders, *Fundamentals of Acoustics*, fourth ed., Wiley, New York, 2000 pp. 284–286 (Chapter 10).
[14] P.A. Nelson, S.J. Elliott, *Active Control of Sound*, Academic Press, New York, 1992.
[15] F.J. Fahy, C. Schofield, Note on the interaction between a Helmholtz resonator and an acoustic mode of an enclosure, *Journal of Sound and Vibration* 72 (3) (1980) 365–378.
[16] W.H. Press, *Numerical Recipes in C: The Art of Scientific Computing*, second ed., Cambridge University Press, Cambridge, 1992.
[17] D.K. Anthony, S.J. Elliott, A comparison of three methods of measuring the volume velocity of an acoustic source, *Journal of Audio Engineering* 39 (5) (1991) 355–365.